

Laboratory simulations of astrophysical jets

Sergey V. Lebedev¹, Francisco Suzuki-Vidal¹, Andrea Ciardi^{2,3},
Matteo Bocchi¹, Simon N. Bland¹, Guy Burdiak¹,
Jerry P. Chittenden¹, Phil de Grouchy¹, Gareth N. Hall¹,
Adam Harvey-Thompson¹, Alberto Marocchino¹, George Swalding¹,
Adam Frank⁴, Eric G. Blackman⁴ and Max Camenzind⁵

¹The Blackett Laboratory, Imperial College London, SW7 2BW London, UK
email: s.lebedev@imperial.ac.uk

²LERMA, Université Pierre et Marie Curie, Observatoire de Paris, Meudon, France

³École Normale Supérieure, Paris, France. UMR 8112 CNRS

⁴University of Rochester, Department of Physics and Astronomy, Rochester, NY, U.S.A.

⁵University of Heidelberg, Centre for Astronomy Heidelberg (ZAH), Landessternwarte
Koenigstuhl D-69117, Heidelberg, Germany

Abstract. Collimated outflows (jets) are ubiquitous in the universe, appearing around sources as diverse as protostars and extragalactic supermassive black holes. Jets are thought to be magnetically collimated, and launched from a magnetized accretion disk surrounding a compact gravitating object. We have developed the first laboratory experiment to address time-dependent, episodic phenomena relevant to the poorly understood jet acceleration and collimation region (Ciardi *et al.*, 2009). The experiments were performed on the MAGPIE pulsed power facility (1.5 MA, 250 ns) at Imperial College. The experimental results show the periodic ejections of magnetic bubbles naturally evolving into a heterogeneous jet propagating inside a channel made of self-collimated magnetic cavities. The results provide a unique view of the possible transition from a relatively steady-state jet launching to the observed highly structured outflows.

Keywords. ISM: jets and outflows, hydrodynamics, plasmas, methods: laboratory

1. Introduction

The scaled study of astrophysical phenomena in laboratory experiments has seen major advances in recent years due to developments in the field of high-energy-density physics. The generation of extreme states of matter involving high temperatures (110 keV), densities ($10^{-5} 10^1 \text{ g/cm}^3$), and velocities (few $\times 100 \text{ km/s}$) provides either a direct link to the physics encountered in a variety of astrophysical objects or a scaled representation of astrophysical dynamics, such as jets (see Ref.2 Remington *et al.*, 2006 for a review).

Although jets and outflows are associated with widely diverse astrophysical environments, they exhibit many common features independent of the central source (Livio, 2002). In all contexts, jets are believed to be driven by a combination of magnetic fields and rotation via, in most cases, an accretion disk (Lovelace, 1976, Blandford & Payne, 1982, Ferreira, 1997, Ouyed *et al.*, 1997). The standard magnetohydrodynamic jet models rely on rotation to twist a large-scale poloidal magnetic field B_P , producing a toroidal field B_Φ that drives and collimates the outflow. Our experiments are designed to model the acceleration and collimation of astrophysical jets taking place under the initial conditions $|B_\Phi| \gg B_P$. The experiments also apply to magnetic tower models (Lynden-Bell, 1996, Nakamura *et al.*, 2007), where differential rotation of closed magnetic field lines creates a highly wound magnetic field which drives a magnetic cavity as well as collimating a jet on its axis. How jets survive such unstable field configurations is one of the

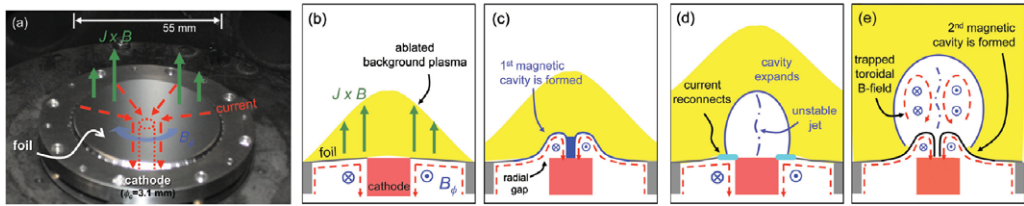


Figure 1. (a) A radial foil inside the discharge chamber of MAGPIE, with the cathode shown schematically (not to scale). (b) Schematic showing the mechanism of episodic magnetic cavity formation triggered by current reconnection at the base of the cathode. In both figures the current path (red-dashed arrows), toroidal magnetic field (blue arrows) and the resultant $\mathbf{J} \times \mathbf{B}$ force (green arrows) are shown

open astrophysical issues addressed by the experiments. Another aspect is the origin of the spatial and temporal variability that is observed on all scales in stellar jets (Hartigan *et al.*, 2005), and which is often interpreted as perturbations to a relatively steady flow.

By performing appropriately scaled, high-energy density plasma experiments, extreme laboratory astrophysics has recently emerged as a novel approach to complement our understanding of complex astrophysical phenomena (see Remington *et al.*, 2006 for a review). Jets have been the subject of several studies, which may be distinguished (Blackman, 2007) by whether they addressed problems related to the propagation (e.g. Foster *et al.*, 2005, Ciardi *et al.*, 2008), the launching (Hsu & Bellan, 2002), or both (Lebedev *et al.*, 2005, Ciardi *et al.*, 2007). Here, we present the first laboratory experiments exploring episodic, magnetohydrodynamic (MHD) jets.

Astrophysical jets and outflows are described to first approximation by ideal MHD and our experiments are designed to produce flows in that regime. Its applicability requires the dimensionless Reynolds (Re), magnetic Reynolds (Re_M), and Peclet (Pe) numbers to be much larger than unity; this implies that the transport of momentum, magnetic fields, and thermal energy, respectively, occurs predominantly through advection with the flow. It is important to stress that astrophysical jets have typical values $Re > 10^8$, $Re_M > 10^{15}$, and $Pe > 10^7$ that are many orders of magnitude greater than those obtained not only in the laboratory but also in numerical simulations, which have been so far the sole means of investigating time-dependent behavior of multi-dimensional MHD jets. In ideal MHD simulations, unphysical dissipation occurs at the grid level through numerical truncation errors (Ruy *et al.*, 1995, Lesaffre & Balbus, 2007). For global jet models, mostly performed assuming axisymmetry, the effective numerical Reynolds numbers are typically in the range of $Re_M \sim 10 - 10^3$ (see for example Goodson & Winglee, 1999), and we expect $Re \sim Pe \sim Re_M$. Severe limitations also exist in the range of plasma β , the ratio of thermal to magnetic pressure, which may be reliably modeled numerically (Miller & Stone, 2000). The (inherently) three-dimensional, scaled experiments discussed here extend the range of the dimensionless parameters obtained in the global modeling of jets. Typical values obtained are $Re \sim 5 \times 10^5 - 10^6$, $Re_M \sim 150 - 500$, $Pe \sim 20 - 50$, and $\beta \sim 10^{-3} - 10^3$; the plasma is highly collisional, and the fluid MHD approximation is a valid model. Finally, similar to astrophysical jets, the laboratory flows produced are radiatively cooled.

2. Experimental Setup

The experimental configuration (Fig. 1) is similar to the radial wire array z-pinch used in our previous experiments (Lebedev *et al.*, 2005b). In the present experiments the

current from the MAGPIE generator (peak current of 1.5MA in 250 ns) (Mitchell *et al.*, 1996) is driven into a 6–6.5 μm thick aluminum foil, which is held radially between two concentric electrodes (Fig. 1). The central electrode (cathode) is a hollow cylinder with a diameter of 3.1mm, with the diameter of the outer electrode being 60 mm. Diagnostics included: laser probing ($\lambda = 532 \text{ nm}$, $\delta t \sim 0.4 \text{ ns}$) providing 2-frame interferometry, shadowgraphy and schlieren imaging; time resolved ($\sim 2 \text{ ns}$ exposure) pinhole cameras which recorded emission in the XUV region ($> 30\text{eV}$) providing up to 8 frames per experiment; magnetic pick-up probes to measure any trapped magnetic field inside the outflows; an inductive probe connected to the cathode to measure voltage and thus Poynting flux driving the outflow. The imposed current path (Fig. 1) produces a toroidal magnetic field B_ϕ below the foil which is directly proportional to the current and decreases with the radial distance from the cathode ($B_\phi \propto I(t)/r$). For peak current the toroidal magnetic field can reach magnitudes of $B_\phi \sim 100T$ (1MG) at the cathode radius.

A schematic diagram of the evolution of a typical experimental jet/outflow is shown in Figure 1. Two outflow components are generally present: a magnetic bubble (or cavity) accelerated by gradients of the magnetic pressure and surrounded by a shell of swept up ambient material, and a magnetically confined jet on the interior of the bubble. The confinement of the magnetic cavity itself relies on the presence of an external medium. The dynamics of the first magnetic bubble and jet are similar to those described in (Lebedev *et al.*, 2005b, Ciardi *et al.*, 2007). In the present work, however, we are able to produce and observe for the first time an episodic jet activity. The main difference with our previous experiments is an increased mass, as a function of radius, being available in the plasma source. The initial gap (see Figure 1) produced by the magnetic field is smaller and can be more easily refilled by the readily available plasma. Its closure allows the current to flow once again across the base of the magnetic cavity, thus re-establishing the initial configuration. When the magnetic pressure is large enough to break through this newly deposited mass, a new jet/bubble ejection cycle begins.

3. Experimental Results

3.1. Distribution of the Ablated Plasma Above the Foil

The distribution of plasma ablated from the foil and the initial axial motion of the foil were measured from side-on laser probing images. An example of a laser interferogram obtained at 172 ns after the start of the current pulse in Fig. 2a, where the bulk motion of the foil is seen as a dark non-transparent region above its initial position. The axial displacement increases at smaller radius, which is consistent with a larger magnetic pressure as radius decreases.

Above the boundary it is possible to measure the electronic density of the plasma by following the fringe shift of the interferogram. Fig. 2b shows a 2-D map of integrated electronic density across the plasma $\int n_e(r, z)dL \simeq n_e L$ obtained from the analysis of Fig. 2a, performed with the IDEA interferometric software (Hipp *et al.*, 2004). The contours in this figure represent regions of constant values of $n_e L$. Most of the plasma is concentrated in the region above the cathode, decreasing with distance from the axis. This agrees with a larger ablation rate of plasma at smaller radius, where the Lorentz $\mathbf{J} \times \mathbf{B}$ force is the strongest. The good degree of azimuthal symmetry in the ablated plasma allowed obtaining the radial electronic density $n_e(r)$ by using Abel inversion technique. Radial profiles at of $n_e L$ at different heights from the foil ($z=1, 1.3, 2, 3$ and 3.5 mm) are shown in Fig. 2c, with their respective Abel-inverted profiles in Fig. 2d. By integrating these profiles along the radius and assuming a value for the ionization of the plasma it is possible

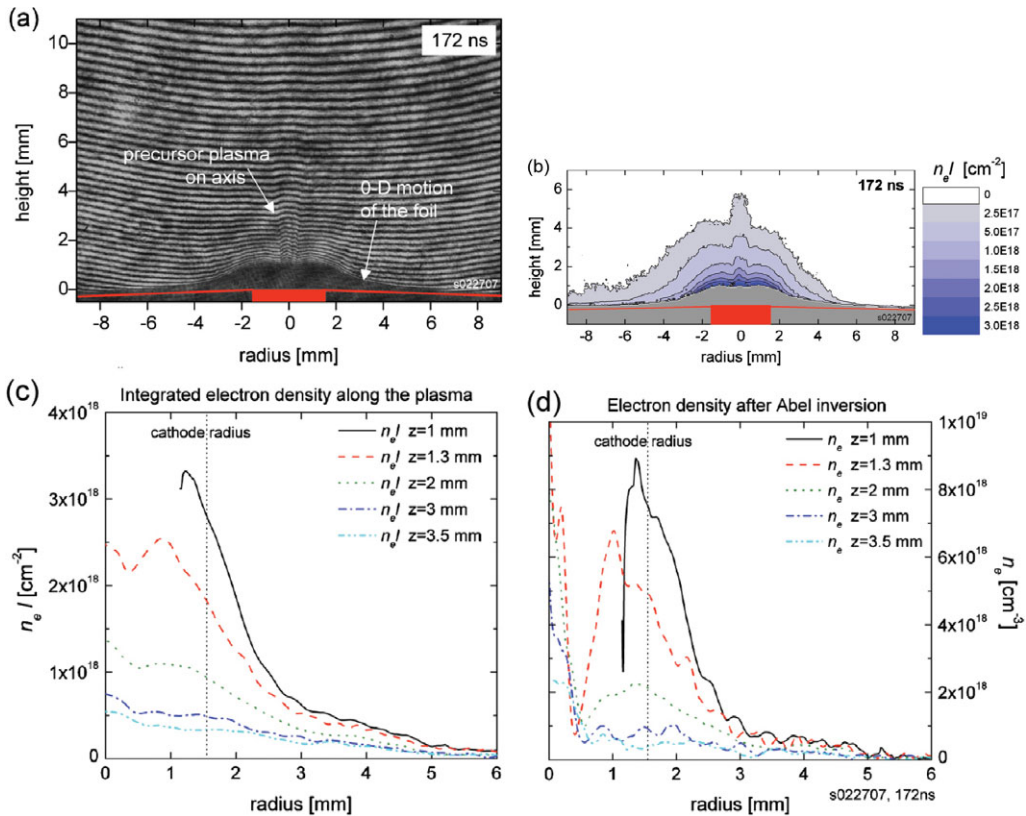


Figure 2. (a) Side-on laser interferogram at 172 ns showing the axial displacement of the foil (dark region) in respect to its initial position (red dotted lines) before the start of the current (the cathode is shown in red). Bending of the interference fringes is due to the plasma expanding from the foil and a hydrodynamic jet on axis. (b) 2-D map of electronic density, integrated along the line of sight $n_e L$ reconstructed from Fig. 2a. (c) Profiles of $n_e L$ as a function of radius at different heights above the foil and (d) the corresponding Abel-inverted electronic density profiles n_e .

to estimate the mass ablated from the foil at this time, which results in $< 1\%$ of the total mass from the foil inside a radius of 3 mm. At this time plasma is seen to expand to a maximum height of $z \sim 6$ mm. Assuming that plasma is formed at the start of the current pulse this results in an axial expansion velocity of $V_z \sim 35$ km/s. An interesting feature of the ablated plasma motion above the foil is the formation of a precursor plasma jet on the axis of the foil, which is seen in Fig. 2 as an increase of the electronic density in the region above the cathode. This jet is formed from the plasma which is redirected towards the axis by radial pressure gradients, as there is no ablation above the cathode, which initially leaves an empty region on the axis. The converging towards the axis plasma flow forms a standing shock which redirects the flow in the vertical direction, forming a plasma jet. The formation of this "hydrodynamic" plasma jet is similar to jet formation in our previous experiments with conical wire arrays (Lebedev *et al.*, 2002). The dynamics of the interaction of this hydrodynamic jet with an ambient gas introduced above the foil is relevant to the modeling of jet-ambient interaction, and first results of such experiments are presented in (Suzuki-Vidal *et al.*, 2009).

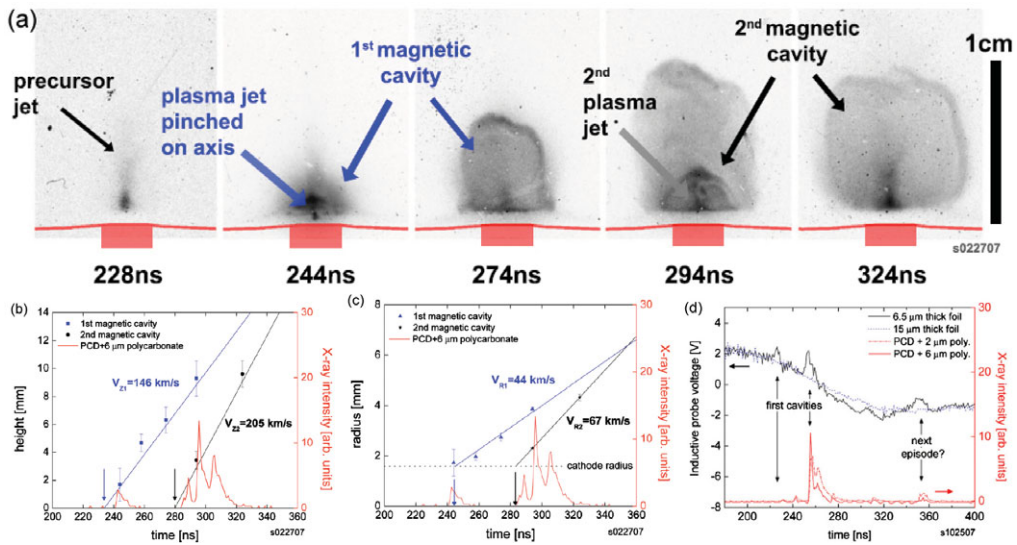


Figure 3. (a) Sequence of side-on XUV emission images showing the formation of two subsequent magnetic cavities during the same experiment. The initial positions of the foil and the cathode (with a diameter of 3.1 mm) are shown schematically. (b)-(c) Measured maximum height and radius of the two magnetic cavities from (a). The X-ray emission is also shown (in red). (d) Top: Voltage signals from an inductive probe from a 6.5 μm thick (solid black) and 15 μm thick (dashed blue) foils. Bottom: X-ray emission from a 6.5 μm thick foil, which is correlated to rapid changes in inductance

3.2. Formation and Dynamics of Episodic Jets

The formation of magnetically driven jets starts later in time, when the Lorentz $\mathbf{J}_R \times \mathbf{B}_\Phi$ force (which is strongest at the cathode radius) leads to ablation of all of the foil mass near the cathode and to the formation of a small radial gap between the cathode and the remainder of the foil. From this moment the Poynting flux can be injected through this gap into the region above the foil. The toroidal magnetic field pushes the ablated plasma axially and radially outwards and also pinches the plasma on axis, forming a magnetic tower jet configuration. At this stage the current flows along the jet on the axis of the magnetic cavity and along the walls of the cavity, in the same way as in our previous experiments (Lebedev *et al.*, 2005b, Ciardi *et al.*, 2007). The magnetic pressure from these rising toroidal loops inside the cavity inflates it both radially and axially, with measured velocities of $V_R \sim 50 - 60 \text{ km/s}$ and $V_Z \sim 130 - 200 \text{ km/s}$ respectively. Experimental results demonstrating such dynamics are shown in Fig. 3. The first cavity shows a high emitting region on the axis, which can be identified as pinching of plasma. It can be seen that the initial diameter of the bubble is given by the diameter of the cathode. The most prominent feature of this new experimental set-up is that we now observe several subsequent outflows formed in the same experiment. It is possible to follow the axial positions of the subsequent episodes of the outflows shown in Fig. 3, with Fig. 3b presenting the measurements that allowed the determination of their velocities along the axis. It is seen that each outflow is expanding with approximately constant velocity, and the extrapolation of the trajectories back in time allows determining the starting time for each episode. The second bubble expands with a faster velocity, $V_Z = 205 \text{ km/s}$ while the first with only 145 km/s . This increase in velocity is consistent with sweeping of the ambient plasma by the earlier episode, thus allowing the subsequent

magnetic bubbles to propagate through a lower ambient density. Up to five subsequent magnetically driven cavities were observed (Ciardi *et al.*, 2009, Suzuki-Vidal *et al.*, 2009). Figure 3b also shows that the episodic outflows are accompanied by episodic outbursts of soft X-rays (detector sensitive to photon energy between 200–300 eV and above 800 eV), which can be well correlated with the formation of each new magnetic tower jet. This is an indication that each new episode starts from the pinching of plasma on the axis of the magnetic cavity and that pinched plasma is the source of the X-ray emission. Both the axial expansion dynamics and the periodicity of X-ray emission show a timescale of ~ 30 ns for the formation of subsequent magnetic tower outflows. The fast rising (~ 5 ns) part and peak of the emission are related to the maximum compression of the jet. We measured jet temperatures up to ~ 300 eV using spatially resolved, time-integrated spectroscopic measurements of H-like to He-like line ratios (Ciardi *et al.*, 2009). Typical flow velocities observed are $\sim 100 - 400$ km/s, the simulated sonic and the Alfvénic Mach numbers in the jet, defined as the ratios of the flow speed to the sound and Alfvén speed, respectively, are $M_S \sim M_A \sim 3 - 10$.

The voltage responsible for reconnection of current across the radial gap between the cathode and the leftover foil is induced by the dynamics of the magnetic cavity and was measured using an inductive voltage probe. The voltage measured by this probe is proportional to the time derivative of the magnetic flux produced by the current from the cathode and along the foil, connecting to ground. Thus the probe voltage V_{ind} is equal to $V_{ind} = -d(LI)/dt$, where the inductance L is related to the current path. An example of the inductive voltage probe signal obtained in a different experiment is shown in Fig. 3d, where the voltage signal from a standard $6.5 \mu\text{m}$ thick foil is compared with a reference shot, in which a foil with a thickness of $15 \mu\text{m}$ was used. In the case of the reference shot the foil did not move on the time-scale of the experiment, the inductance was constant and measured voltage was equal to $V_{ind} = -LdI/dt$.

For the case when the episodic jets were produced, for a $6.5 \mu\text{m}$ foil, the inductive probe shows rapid changes in voltage in respect to the reference case, as seen at ~ 220 , 250 and 290 ns. The timing of these voltage spikes agrees with the X-ray emission measured in the experiment (shown at the bottom of Fig. 3d). The deviations of the voltage from the reference case come from an additional inductance due the change in the current path as the current now flows through the central jet returning along the wall of the cavity. This inductance is time dependent as the cavities expand and the jet is pinched. Fig. 3d also shows that the inductive probe voltage is correlated to the X-ray emission pulses, which are in turn correlated to the formation of two subsequent magnetic cavities seen from the imaging diagnostics. The use of an inductive probe allowed to measure the inductance associated with the formation of a magnetic cavity and thus to obtain estimates the energy balance during an episode, i.e. magnetic energy and Poynting flux. The electromagnetic energy delivered to a typical bubble via Poynting flux is ~ 800 J, and we estimate the kinetic energy of the flow to be $\sim 100 - 400$ J, the remainder is in the magnetic energy, internal energy of the plasma and partly lost to radiation. These results indicate that $\sim 25\%$ of Poynting flux energy entering the magnetic cavity is converted into kinetic energy of the outflow. Details on these measurements will be presented in future publications.

The temporal evolution of the jets and bubbles on the longer time-scale is presented in Figure 4. A succession of multiple cavities and embedded jets are seen to propagate over length scales spanning more than an order of magnitude. The resulting flow is heterogeneous and clumpy, and it is injected into a long-lasting and well-collimated channel made of nested cavities. It is worth remarking that the bow-shaped envelope is driven by the magnetic field and not hydrodynamically by the jet.

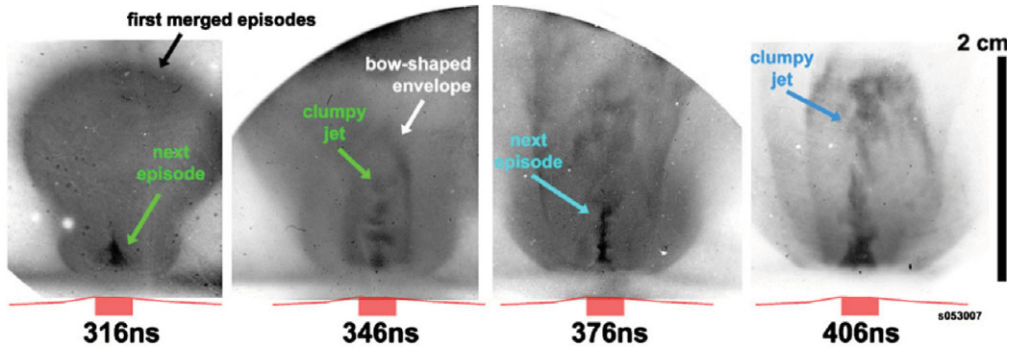


Figure 4. Time series of filtered XUV emission images showing late-time evolution of episodic jets

3.3. Trapped magnetic field inside a magnetic cavity

The estimates presented above show that the magnetic Reynolds number Re_M is much greater than unity and some magnetic flux should remain trapped inside the outflows. In particular, we can expect conservation of magnetic flux accumulated in the first cavity by the time the second cavity starts to form. The presence of toroidal magnetic field inside the expanding magnetic cavities was measured with a magnetic probe. The probe had five circular turns of 3 mm diameter and it was placed 10 mm above the foil at a radial distance of ~ 13 mm from the axis, as shown in Fig. 5. The probe orientation was such that it measured the toroidal component of the magnetic field. To exclude capacitive coupling between the probe and the cathode and also to prevent possible electron flow from the cathode region reaching the probe, a 1 mm thick stainless steel diaphragm was installed at $z \sim 2$ mm above the foil. The magnetically driven jets were formed through a 10 mm diameter aperture in the diaphragm.

An XUV emission image in Fig. 5(b) shows two magnetic cavities expanding above the metallic diaphragm. The position of the cathode, the diaphragm, and the circular aperture on the axis are shown schematically in this figure. The position of the magnetic probe can also be seen from this image as a circular emitting boundary, due to the interaction of its outer shielding with the expanding cavity. This image shows that the addition of the probe and the diaphragm did not affect the overall dynamics of episodic jet formation.

The voltage measured by the magnetic probe is shown in Fig. 5(c). It can be seen that the voltage is zero until ~ 350 ns, which is consistent with the time when the magnetic cavity reaches the probe as seen from imaging diagnostics. The expected response of the magnetic probe assuming a sharp boundary for the toroidal magnetic field inside the expanding bubble can be calculated by taking into account the geometry of the probe and the dynamics of the radial expansion of the cavity, as shown in Fig. 5(b). For the relatively small size of the probe, we can assume that the wall of the magnetic cavity passing the probe at distance $R_B(t)$ from the axis is planar. When the wall of the cavity reaches the probe, the trapped toroidal magnetic field inside the expanding cavity $B_{\Phi, trap}$ will induce a voltage in the probe from the change in the magnetic flux Φ

$$V_{probe} = -\frac{d\Phi}{dt} = -\frac{d[B_{\Phi, trap}(t) \cdot S(t)]}{dt} \quad (3.1)$$

where $S(t)$ is the cross-section area of the probe inside the cavity, related to the radial expansion velocity of the cavity V_R . The radial expansion velocity of the magnetic cavity

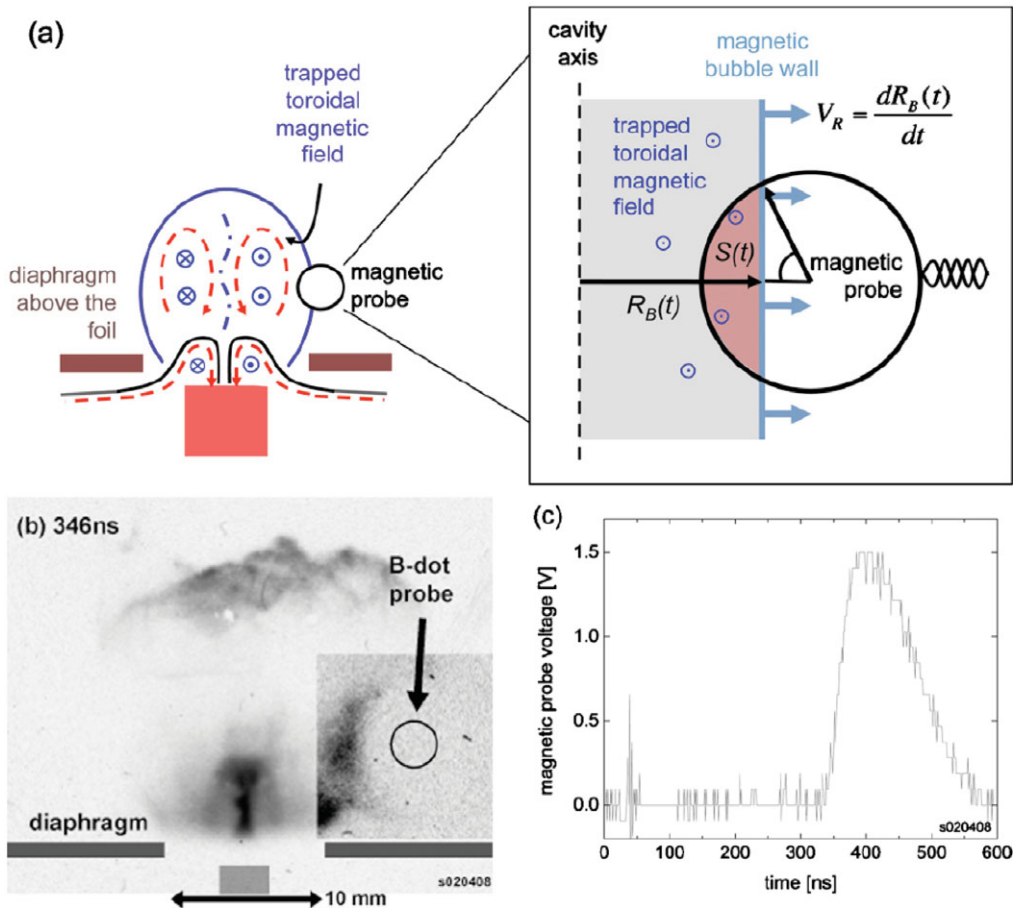


Figure 5. (a) Schematic setup of a radial foil with the addition of a magnetic probe and a metal diaphragm. (b) XUV emission at 346 ns and (c) signal from the magnetic probe obtained in the same experiment

for the particular shot presented in Fig. 5(b) was measured as $V_R \sim 90 \text{ km/s}$, thus corresponding to a signal from the magnetic probe of $B_{\Phi, \text{trap}} \sim 0.3 \text{ T}$.

This estimate can be compared with the expected magnetic field in the expanded magnetic cavity, assuming that the toroidal magnetic flux present in the first cavity at the start of second cavity formation is conserved. The expected magnetic field ($B_{\Phi} \sim 1.5 \text{ T}$) is of the right magnitude, though an accurate estimate of the expected field is not possible due to the uncertainty of the current loop inside the cavity at the time when it reaches the magnetic probe. To improve this comparison, spatially resolved measurements of the magnetic field inside the cavity are needed and three-dimensional MHD simulations (Ciardi *et al.*, 2009) indicate that the initially toroidal magnetic field becomes entangled due to the development of the kink mode of current-driven instability.

4. Summary

In this paper, we have presented results from high energy density plasma experiments designed to investigate the physics of magnetically driven, supersonic, radiatively cooled plasma jets. The most important new feature that appears in the radial foil configuration

is the generation of several subsequent episodes of magnetically driven jets. The formation of the first outflow is similar to that previously observed in the radial wire array configuration. The outflow consists of a jet accelerated and confined by a toroidal magnetic field and embedded in a magnetic cavity. The cavity expansion into the surrounding ambient plasma is driven by the magnetic pressure. Reconnection of the current at the base of the cavity via a plasma expanding from the central electrode and the remnants of the foil leads to the start of the formation of the next outflow episode. The generation of several episodes is reproducible in the experiments and up to three to four eruptions are observed. The formation of each episode is correlated with a burst of x rays from the compressed/pinched jet on the axis.

The key dimensionless parameters Pe , Re , and Re_M are much greater than unity and, together with the Mach number and plasma beta, are all in the astrophysically appropriate regime, which makes the results of the experiments relevant to understanding the physics of launching mechanisms of astrophysical jets. The estimated values of the magnetic Reynolds number in these experiments, $Re_M \sim 200 - 1000$, are comparable or exceed those obtained in global numerical MHD simulations of astrophysical jets. The high values of the magnetic Reynolds number allowed to observe convection/trapping of the toroidal magnetic flux by the. The long term evolution of jets from radial foils might help addressing questions about the spatial and temporal variability of astrophysical jets. In our experiments, the formation of a clumpy jet is the result of the development of current-driven instabilities, which occur within the formation of the episodic ejections. The time variability in the experiments is characterized by two timescales of interest. The first is the growth time of the current-driven MHD instabilities of the order of a few nanoseconds in the experiments. The second is the relatively longer magnetic cavity ejection period of ~ 30 ns. The ratio of both timescales are in the similar regime to those observed in protostellar jets (Ciardi *et al.*, 2009). The episodic formation of magnetically driven jets observed in the experiments allows us to speculate that an episodic scenario of jet formation could be also applicable to the formation of astrophysical jets. Indeed, steady jets confined by a toroidal magnetic field should be highly unstable to current-driven instabilities, unless stabilized by, e.g., a closely positioned rigid "wall" acting as a path for the return current. In the episodic jet formation scenario, the time for the growth of the current-driven modes is reduced to roughly the duration of one episode. The development of the instability could produce, as in the experiments, a clumpy outflow which still retains a high degree of collimation and propagates ballistically after the end of the episode. The resulting outflow in this scenario would have density and velocity variations due to both the current-driven instability and the episodicity of the ejection. We should note that episodic jet formation appeared in several numerical simulations of young stellar objects (YSO) jet launching (Goodson *et al.*, 1997, Goodson & Winglee, 1999, Goodson *et al.*, 1999b, Romanova *et al.*, 2006).

Acknowledgements

This work was supported by the EPSRC Grant No. EP/ G001324/1, by the NNSA under DOE Cooperative Agreement Nos. DE-F03-02NA00057 and DE-SC-0001063, and by a Marie Curie RTN fellowship, as part of the JETSET (Jet Simulations, Experiments and Theories) project.

References

- Blackman, E. G., 2007, *A&SS*, 307, 7
 Blandford, R. D. & Payne, D. G. 1982, *MNRAS*, 199, 883

- Ciardi, A., Lebedev, S. V., Frank, A., Blackman, E. G., Chittenden, J. P., Jennings, C. J., Ampleford, D. J., Bland, S. N., Bott, S. C., Rapley, J., Hall, G. N., Suzuki-Vidal, F. A., Marocchino, A. Lery, T., & Stehle C. 2007, *Physics of Plasmas*, 14, 056501
- Ciardi, A., Ampleford, D. J., Lebedev, S. V., & Stehle C., 2008, *The Astrophysical Journal*, 678, 968-973
- Ciardi, A., Lebedev, S. V., Frank A., *et al.* 2009, *The Astrophysical Journal*, 691, L147-L150
- Ferreira, J. 1997, *A&A*, 319, 340
- Foster, J. M., Wilde, B. H., Rosen, P. A., Williams, R. J. R., Blue, B. E., Coker, R. F., Drake, R. P., Frank, A., Keiter, P. A., Khokhlov, A. M., Knauer, J. P., & Perry, T. S. 2005, *The Astrophysical Journal*, 634, L77-L80
- Goodson, A. P., Winglee, R. M., & Böm, K. H. 1997, *The Astrophysical Journal*, 489, 199
- Goodson, A. P. & Winglee, R. M. 1999, *The Astrophysical Journal*, 524, 159
- Goodson, A. P., Böm, K. H., & Winglee, R. M., 1999, *The Astrophysical Journal*, 524, 142
- Hartigan, P. *et al.* 2005, *Astronomical Journal*, 130, 2197
- Hipp, M., Woisetschlaeger, J., Reiterer, P., & Neger, T., 2004, *Measurement*, 36, 53-66
- Hsu S.C., Bellan, P. M., 2002, *MNRAS*, 334, 257
- Lebedev, S. V., Chittenden, J. P., Beg, F. N., *et al.* 2002, *The Astrophysical Journal*, 564, 113-119
- Lebedev, S. V., Ciardi, A., Ampleford, D. J., *et al.* 2005, *Plasma Physics and Controlled Fusion*, 47, B465-B479
- Lebedev, S. V., Ciardi, A., Ampleford, D. J., *et al.* 2005, *MNRAS*, 361, 97-108
- Lesaffre, P. & Balbus, S. A., 2007, *MNRAS*, 381, 319
- Livio, M. 2002, *Nature*, 417, 125
- Lovelace, R. V. E., 1976, *Nature*, 262, 649
- Lynden-Bell, D., 1996, *MNRAS*, 279, 389
- Miller, K. A. & Stone, J. M. 2000, *The Astrophysical Journal*, 534, 398
- Mitchell, I. H., Bayley, J. M., Chittenden, J., *et al.* 1996, *Rev. Sci. Instr.*, 67, 1533-1541
- Nakamura, M., *et al.* 2007, *The Astrophysical Journal*, 656, 721
- Ouyed, R., *et al.* 1997, *Nature*, 385, 409
- Remington, B. A., Drake, R. P., & Ryutov, D. D., 2006, *Review Modern Physics*, 78, 755
- Romanova, M. M., Kulkarni, A., Long, M., *et al.* 2006, *Adv. Space Res.*, 38, 2887
- Ryu, D., *et al.* 1995, *The Astrophysical Journal*, 452, 785
- Suzuki-Vidal, F., Lebedev, S. V., Ciardi, A., *et al.* 2009, *Astrophysics and Space Science*, 322, 19-23